INTERFACE

rsif.royalsocietypublishing.org

Research

Cite this article: Ebihara R, Hashimoto H, Kano J, Fujii T, Yoshioka S. 2018 Cuticle network and orientation preference of photonic crystals in the scales of the weevil *Lamprocyphus augustus*. *J. R. Soc. Interface* **15**: 20180360.
http://dx.doi.org/10.1098/rsif.2018.0360

Received: 19 May 2018
Accepted: 13 July 2018

Subject Category:
Life Sciences–Physics interface

Subject Areas:
biophysics

Keywords:
structural colour, photonic crystal, weevil

Author for correspondence:
S. Yoshioka
e-mail: syoshi@rs.tus.ac.jp

Electronic supplementary material is available online at https://dx.doi.org/10.6084/m9.figshare.c.4174832.

THE ROYAL SOCIETY PUBLISHING

Cuticle network and orientation preference of photonic crystals in the scales of the weevil *Lamprocyphus augustus*

R. Ebihara[1], H. Hashimoto[2], J. Kano[3], T. Fujii[3] and S. Yoshioka[1]

[1]Department of Physics, Faculty of Science and Technology, Tokyo University of Science, 2641 Yamazaki, Noda 278-8510, Japan
[2]Department of Applied Chemistry, School of Advanced Engineering, Kogakuin University, 2665-1 Nakano, Hachioji, Tokyo 192-0015, Japan
[3]Graduate School of Natural Science and Technology, Okayama University, Okayama 700-8530, Japan

SY, 0000-0002-7347-2864

This paper reports the structural and optical investigations of the structural colour of the weevil *Lamprocyphus augustus*. The photonic crystal structure within the weevil's scales was investigated using sequential focused ion-beam milling and scanning electron microscopy imaging. We carefully analysed the reconstructed three-dimensional structure to determine the unit cell of the photonic crystal. It was found that the cuticle network of the cubic unit cell perfectly matches the previously reported diamond-based network. However, different results were obtained for the crystal orientations of the small crystal domains that comprise the entire photonic crystal structure in the scales: <111> directions are highly preferred along the surface normal of the scale. This finding explains the fact that the scale is almost uniformly coloured despite the multi-domain structure. It is confirmed experimentally and theoretically that the wavelength range of the reflection band corresponds to the gap of the photonic band.

1. Introduction

Brilliantly coloured butterflies and weevils are probably the most famous examples of insects that use the photonic crystal structure for coloration [1,2]. The scales on the butterfly's wing and the weevil's elytron have a three-dimensional (3D) network of cuticles that are periodic, with the size comparable with the wavelength of light. These insects are interesting not only because they are natural examples of photonic crystals, which have attracted a considerable amount of attention for decades [3], but also because the understanding of the formation process may reveal a novel self-organizing method for photonic crystal production.

The determination of the type of structure to investigate the optical properties of photonic crystals is a fundamental step. Recent studies on the wing scales of several butterfly species have revealed that the cuticle network takes the form of a single gyroid structure [4–6]. On the other hand, various structural types have been reported for weevil scales, and they are summarized well in the supporting information of a previous study [7]. One common way to determine the photonic structure is the pattern matching method, in which the cross-sectional images obtained by transmission electron microscopy are compared with those of theoretical models [4,8]. Small-angle X-ray scatting (SAXS) is another method that has been used to distinguish photonic crystal structures with different Bravais lattices [5,9].

On the other hand, several techniques allow us to observe 3D cuticle networks directly. One is sequential focused ion-beam (FIB) milling and scanning electron microscopy (SEM) imaging, where the 3D structure can be reconstructed from the sequential cross-sectional images [10]. Electron tomography and high-resolution

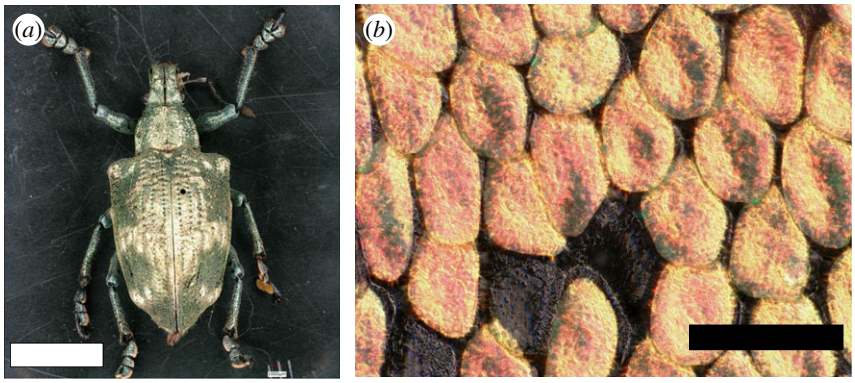

Figure 1. Photographs of (*a*) weevil *Lamprocyphus augustus* and (*b*) scales on the elytron. Scale bar: (*a*) 1 cm and (*b*) 100 µm.

X-ray tomography are the other methods that have been applied to the study of photonic crystals in insects [6,11–14]. These methods provide us with detailed structural information on the cuticle network. However, owing to its complexities, it is not an easy task either to analyse it three dimensionally or to present clear evidence supporting a particular theoretical model. Thus, the analysis often comes back to the two-dimensional (2D) comparison, where the patterns of arbitrary cuts of the reconstructed volume are compared with those of theoretical models [10,11]. Although the 2D agreements show consistencies with a theoretical model, it is difficult to judge how exclusively the model is suggested. Thus, it is desirable to compare the 3D network topology directly, as reported for the wing scale of a butterfly [6].

The photonic crystal consists of a 3D repetition of the unit cell. Thus, the comparison of the unit cell between the experiment and theory can be a direct way for structural characterization. In this paper, we report such an analysis of the scales of the weevil *Lamprocyphus augustus* (figure 1*a*). We are interested in this species because of the following two reasons. Firstly, this weevil is the first insect that has been reported to possess the diamond-based cuticle network structure, which is known to be the champion among photonic crystals that can exhibit a wider photonic band gap [15]: Galusha *et al*. reported [10] that the cuticle network of *L. augustus* is very similar in configuration to a synthetic diamond-based structure [16]. They also compared the 2D morphologies on three orthogonal planes with the theoretical model. However, a recent SAXS study for this weevil species reported both gyroid and diamond structures [9]. Thus, it is meaningful to reinvestigate the photonic crystal structure.

Another reason why we are interested in *L. augustus* is related to the recent findings on the relative crystal orientations of the multi-domain photonic crystals (the degree of the crystallographic texture). In both the butterfly and the weevil, the photonic crystal in the scales is usually separated into many small crystal domains. Interestingly, it has been found in a few butterfly species that the crystal orientations are not perfectly random among the small crystal domains, but there is a preference that a specific crystal orientation is along the surface normal to the scale [13,17–19]. In other words, the crystal orientations can be highly textured. The textured crystal orientation is important because it makes the scales look uniformly coloured despite the multi-domain structure. *L. augustus* is apparently a candidate of the weevil species that has such an orientation preference, because the scales are almost uniformly coloured when many crystal domains are observed in cross section [10].

In this paper, we report the structural and optical investigations of the structural colour of the weevil *L. augustus*. The photonic crystal structure within the scale is investigated by using sequential FIB milling and SEM imaging. The cuticle network is reconstructed three dimensionally, and analysed to determine the cubic unit cell. The morphologies of the photonic crystal surfaces are also investigated to examine whether preferred crystal orientations exist. Optical properties of the scales are investigated experimentally and theoretically by measuring the reflectance spectrum with a microspectrophotometer and by calculating the photonic band structure.

2. Material and methods

Samples of the weevil *L. augustus* were provided by Prof. Helen T. Ghiradella at the University at Albany, State University of New York. The colour pattern of the scales was observed using an optical microscope (Keyence VHX-6000) under epi-illumination (figure 1*b*). Microspectrophotometry was used to determine the reflectance spectrum of a small region within a single scale. The experimental system consisted of an optical microscope (OLYMPUS BX51) and a fibre optic spectrometer (Ocean Optics USB2000) [20]. The objective lens was capable of 50× magnification (OLYMPUS SLMPlan N, NA:0.35) and the fibre diameter was 200 µm, so that a 4 µm diameter region was examined. The reflectance was determined by dividing the observed spectrum by that of a diffuse reflection standard (Labsphere, Spectralon).

For electron microscopy, the scales from the elytra were transferred to a glass slide using a scalpel, and then a single scale was picked up with a thin pulled-glass pipette and attached to a metal sample stage, which was a $6 \times 6 \times 10$ mm^3 cuboid-aluminium block, using a piece of carbon conductive double-faced adhesive tape. We paid attention to placing the scale near the edge of the top surface of the aluminium block to make the following milling procedure easier. We employed an FIB-SEM system (JEOL JIB-4500FE) for the structural investigations. The top cuticle layer covering the internal photonic crystal was first removed by FIB milling and the exposed photonic crystal surface was observed with SEM. Before the FIB milling process, the scale was coated with 2.5 nm thick Os using an Os coater (Meiwafosis Neoc-Pro) to increase conductivity. To mill off only the top cuticle layer, the sample stage was tilted so that the scale surface became parallel to the ion beam. The milling procedure was performed under a beam current of 0.3 nA and accelerating voltage of 15 kV. In some observations, the scale was first cross sectioned by using a razor blade, and then the top cuticle layer was FIB-milled in order to observe the structure from two orthogonal directions.

We employed another stable FIB-SEM system (Helios NanoLab TM 600i) to carry out the sequential FIB milling and SEM imaging (slice-and-view observation). The FIB milling process

was performed under a beam current of 33 pA and accelerating voltage of 30 kV. The slice thickness chosen was 17 nm, which was found to be much smaller than the lattice constant. After the first SEM image was obtained, the slice-and-view process was repeated 79 times, so that the total sliced thickness was 1.34 µm. The 80 SEM images obtained were corrected for the view angle and the drift during the processes, and finally used for 3D rendering. Commercial software (Wolfram Research MATHEMATICA v. 11.1) was used for the rendering, analyses, and theoretical modelling and calculation.

It has been reported for several weevil species that the photonic crystal within the scales can be modelled as the single-diamond network [7,21], which can be approximately expressed by using the following equation:

$$\sin(-X+Y+Z)+\sin(X-Y+Z)+\sin(X+Y-Z)+\sin(X+Y+Z)\le t, \tag{2.1}$$

where $X=(2\pi/a)x$, $Y=(2\pi/a)y$, $Z=(2\pi/a)z$ and x, y, z are Cartesian coordinates. The parameter a is the lattice constant of the cubic unit cell, and t is called a level-set parameter that is related to the volume fraction of the cuticle. The above formula was used as a theoretical model for the photonic crystal.

The photonic band diagram of the diamond photonic crystal was calculated by using the plane-wave expansion method [22]. To calculate the angular frequency of the electromagnetic wave having a wavevector $\boldsymbol{k}$, we expanded the electric and magnetic fields into the plane waves with wavevectors $\boldsymbol{k}+\boldsymbol{G}$, where $\boldsymbol{G}$ denotes reciprocal vectors. We used 2085 reciprocal lattice points around the origin in the reciprocal space. We confirmed that this number was sufficient to obtain the converged results of the calculation.

3. Results

We first examined the colour variation in the scale by measuring the reflectance spectrum with a microspectrophotometer. Thirteen randomly chosen 4 µm diameter regions within a single scale were examined; the results for five of these regions are shown in figure 2. The spectra have a strong reflection band ranging approximately from 550 to 650 nm. The results for the other regions have similar spectral shapes. We calculated the peak wavelength λ_p as the average of the two wavelengths at the half maximum. The average of λ_p of the 13 spectra was found to be 604 ± 11 nm, quantitatively indicating that the yellow-orange colour of the scale is almost uniform. However, the edge of the scale is observed to be green under the microscope, probably due to the tilt of the scale surface. We also examined the polarization effect by using polarizer and analyser and found that the reflection from the scale does not largely change with the polarization.

Next, we investigated the crystal orientation of the photonic crystal domains; the surface cuticle layer was removed by FIB milling and the exposed photonic crystal was directly observed with SEM. The photonic crystal surface appears to consist of a layer of cuticle networks with regularly arranged air holes, as shown in figure 3. As a simple analysis, sets of three white lines are drawn along the cuticle network at several points. The angles between the lines are found to be approximately 60°, suggesting that the (111) surface of the cubic lattice faces the scale surface. The differences in the orientations of the white lines at the different points indicate that the network structure is separated into many crystal domains with different orientations as the domain boundaries are drawn as dashed curves.

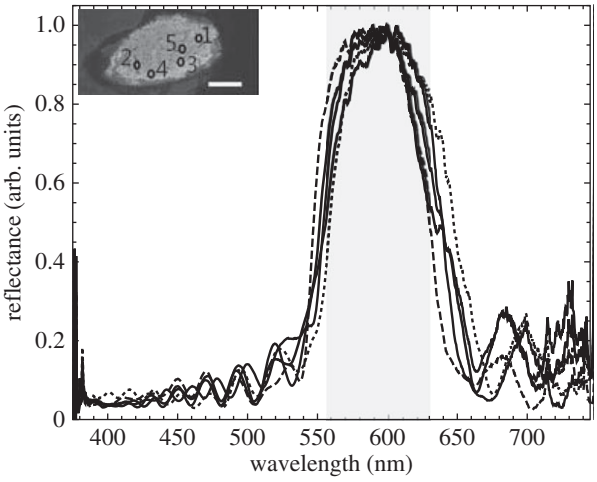

Figure 2. Reflectance spectra determined with the microspectrophotometer for five positions on a single scale. A strong reflection band ranges approximately from 550 to 650 nm. The two spectra having reflection bands centred at the longest and shortest wavelengths are drawn as dashed and dotted curves, respectively, for the clarification. The grey region represents the photonic band gap of the diamond photonic crystal along the Γ-L direction. Upper left inset: the experimentally examined scale with five circles showing the measurement positions. Scale bar, 20 µm.

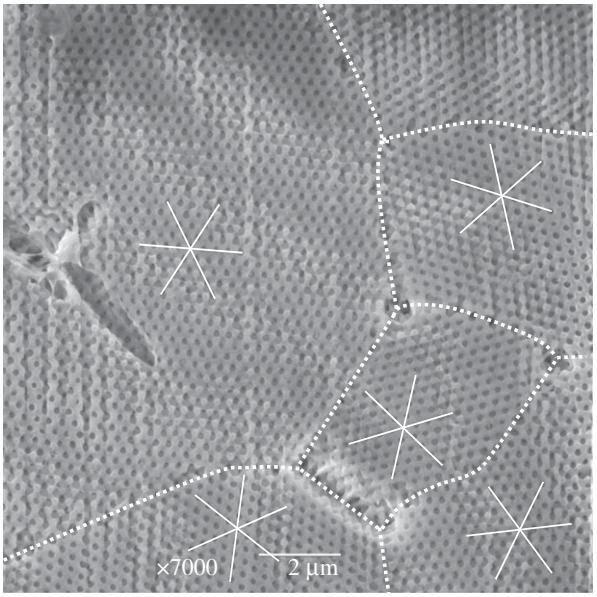

Figure 3. SEM image of the exposed photonic crystals after the surface cuticle layer was removed. Sets of three white lines are drawn along the lines of the cuticle network. Dashed curves are boundaries between the different crystal domains that are drawn according to the difference in the cuticle network orientation.

It should be emphasized that all the crystal domains have surface morphologies with a sixfold symmetry. This fact clearly suggests the strong preference of ⟨111⟩ orientations to be along the surface normal. The previously reported different textures observed in the cross section [10] can be attributed to the differences in the in-plane crystal orientations. To confirm this explanation, we observed the photonic crystals from two orthogonal directions, as schematically illustrated in figure 4*a*. Figure 4*b* shows a part of the scale that includes two crystal domains with a boundary running from the centre of the image bottom to the upper right (dashed line). In the cross section, we can clearly see the different surface

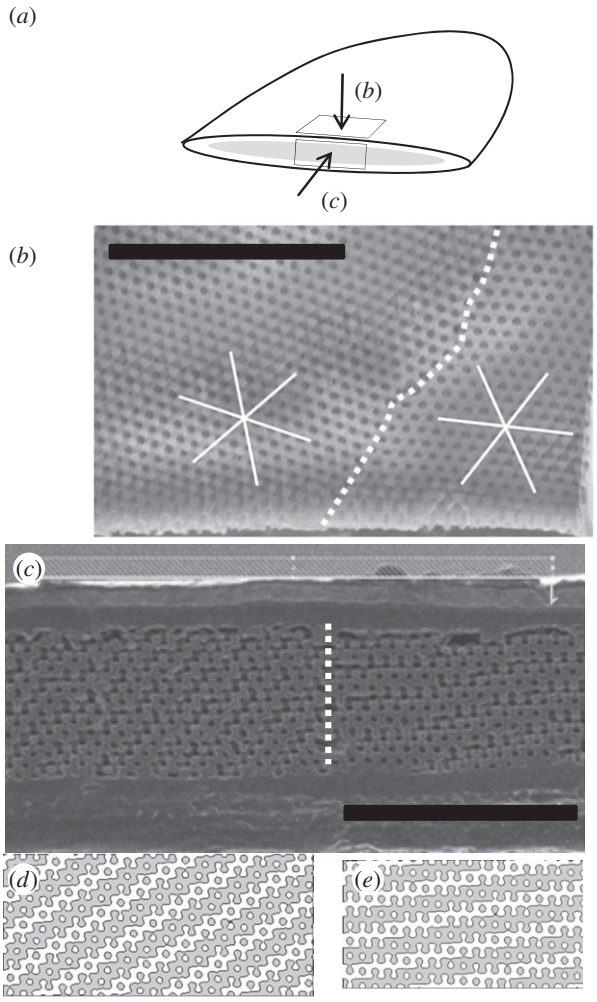

Figure 4. Structural observation from two orthogonal directions. (*a*) Schematic illustration of the observation. (*b*) SEM image of the top surface of the photonic crystal. Sets of three white lines are drawn along the lines of the cuticle network. There is a domain boundary (dashed curve) that runs from the centre of the image bottom to the upper right. Scale bar, 5 µm. (*c*) The cross section of the part corresponding to (*b*). Different surface textures are seen between the left and right crystal domains. The top cuticle layer remains because this observation was made prior to the milling process. Scale bar: 5 µm. (*d*,*e*) Model surface morphologies reproducing the textures in (*c*). They are obtained by assuming the single-diamond photonic crystal structure. The normal vectors of the surfaces are along the $[\bar{6}\ \bar{3}\ 8]$ and $[\bar{5}\ \bar{4}\ 8]$ directions for (*d*) and (*e*), respectively. These directions are nearly perpendicular to the [111] direction.

morphologies corresponding to the two crystal domains, as shown in figure 4*c*. It is confirmed that similar surface morphologies can be reproduced by assuming the diamond photonic crystal structure, as shown in figure 4*d*,*e*, where the normal vector of the cross section is assumed to be nearly perpendicular to the [111] direction.

From the hexagonal arrangement of the air holes, the estimated lattice constant a was 401 nm; an image analysis was conducted to determine the distances between the centres of the neighbouring air holes shown in figure 3, which are found to correspond to $a/\sqrt{2}$ from a simple analysis using equation 2.1. The value of 401 nm is slightly smaller than the previously reported value of 450 nm [10].

Next, we performed sequential FIB milling and SEM imaging and obtained 80 images at every 17 nm height. Figure 5*a* shows the SEM image observed at three different heights with a separation of 238 nm (=17 nm × 14). This height separation is chosen to be almost one-third of the diagonal length of the cubic unit cell ($\sqrt{3}a/3 \approx 231$ nm). Careful inspection reveals that the positions of the air holes shift with the height. The regions of the holes are extracted by using an image binarization process, and they are superimposed as shown in figure 5*b*. It can be clearly seen that the air-hole positions change like the so-called ABC stack, implying that the photonic crystal forms a face-centred cubic lattice.

Finally, we reconstructed a 3D structure of the cuticle network, as shown in figure 6*a*–*c*. We define new spatial coordinates x', y', z' that are along the sides of the rendered volume, as shown in figure 6*a*. In the next section, we analysed three dimensionally the reconstructed structure and compared it with the single-network diamond photonic crystal.

4. Analysis

We have checked that the observed 2D cuticle patterns are consistent with the single-diamond network that is expressed by equation (2.1). To eliminate the ambiguity in the structural identification, we analysed three dimensionally the reconstructed structure to take out the single cubic unit cell and compare it with the theoretical model. For this purpose, we first need to express the ⟨100⟩ directions in terms of the $x'y'z'$ coordinates.

The hexagonal arrangement of the air holes suggests that the z' axis is nearly along the [111] direction. To determine other crystal orientations, we use a unique feature of the single-network diamond photonic crystal: when the crystal structure is viewed from certain directions, air holes appear to penetrate the structure, as shown in figure 6*e*,*f* . There are two groups of such directions that differ in angle from the [111] direction. The first group contains [110], [101] and [001] directions that are at 35.3° from the [111] orientation (figure 6*e*), while the second group contains $[1\bar{1}0]$, $[01\bar{1}]$ and $[\bar{1}10]$ directions that are at 90° from the [111] direction (figure 6*f*). By rotating the rendered volume, we expected to find six such directions, and two of them are shown in figure 6*b*,*c*. As is expected from the above feature, three of the six directions are found to be at approximately 35° (33.6°, 37.5°, 34.2°) from the z' axis, and the other three directions are found to be at approximately 90° (88.2°, 89.6°, 91.8°) from the z' axis. Thus, we can safely assign these six directions to the ⟨110⟩ directions. As a different approach, we tried to find ⟨100⟩ directions directly by focusing our attention on the fourfold symmetry. However, we found it easier to focus on the aforementioned through-hole feature.

Now that ⟨110⟩ orientations have been expressed in terms of $x'y'z'$ coordinates, the vectors along ⟨100⟩ can be unambiguously calculated. Then, we can take out a cubic volume from the reconstructed structure that has the dimension a^3 with its sides parallel to ⟨100⟩ directions. The only adjustable parameter is the position of the cubic volume. As the position was gradually shifted, we compared the cuticle network with the theory and found the best-matched unit cell, as shown in figure 7 (see also an electronic supplementary material, movie S1). It was found that the network topology perfectly matches that of the single-diamond structure; the cuticle is connected to adjacent cells at the eight corners and at the centres of the six surfaces, and there are four points that are fourfold coordinated. Once the position of a unit cell is determined, similar (exactly the same in principle) cuticle

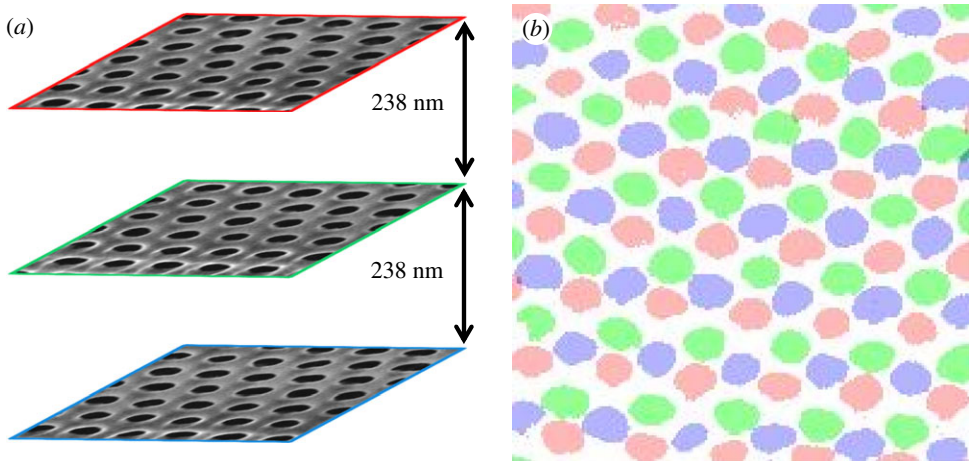

Figure 5. (*a*) SEM images observed at three different heights with a separation of 238 nm. (*b*) The positions of the air holes in (*a*) are superimposed with different colours: red, green and blue from the top to bottom.

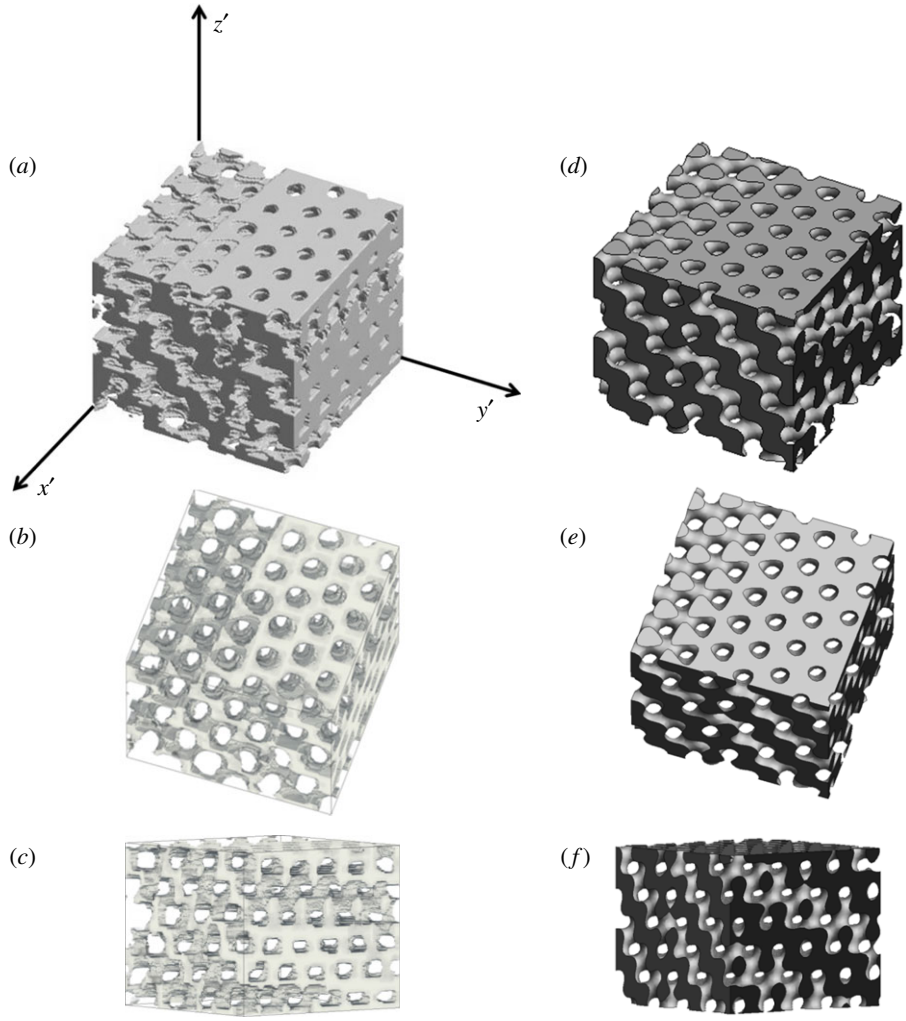

Figure 6. Three-dimensional (3D) structure of the photonic crystal. (*a–c*) The reconstructed structure observed from three different directions. The dimensions of the structure are 1.61 × 1.61 × 1.34 μm^3. In (*a*), the spatial coordinates *x′y′z′* are defined along three orthogonal sides of the rendered volume. In (*b*,*c*), the structure is observed from the directions in which air holes appear to penetrate the structure. The viewing directions are (*a*) (*x′*, *y′*, *z′*)=(2.4,1.3,2.0) , (*b*) (0.51,0.17,0.85) and (*c*) (0.61,0.79,0.07). (*d–f*) The model structure of the diamond photonic crystal that is obtained from the 3D analysis of the reconstructed structure. See text for details. These models are drawn using the parameter as $t = 0.15$ in equation (2.1).

networks should be obtained for the cuboids that are shifted by the primitive translation vectors. It was confirmed that similar networks are observed, as shown in S2, although some of them look slightly distorted. From these results, it can be concluded that the observed cuticle network of *L. augustus* consists of the single-diamond photonic crystal. The reconstructed volume has dimensions 1.61 × 1.61 × 1.34 μm^3, and the crystal orientations of the three orthogonal sides are already known. Thus, we can unambiguously render the diamond photonic crystal structure with corresponding dimensions. We can

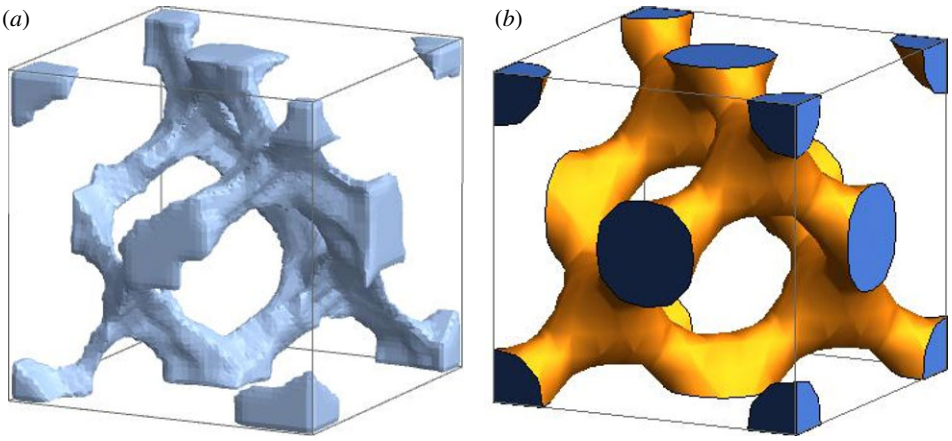

Figure 7. Comparison of cubic unit cell structures. (*a*) A cubic unit cell taken out from the reconstructed structure. To observe the topology more clearly, the cuticle network is made thinner using the Erosion command in Mathematica. (*b*) The cubic unit cell is drawn according to equation (2.1). (Online version in colour.)

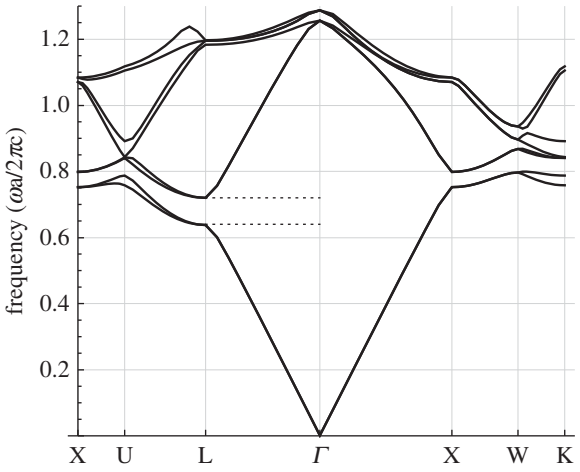

Figure 8. Photonic band diagram of the single-network diamond photonic crystal. The refractive index of the cuticle is assumed to be 1.515 and the level set parameter t in equation (2.1) is assumed to be 0.15. Dotted lines show the frequency range of the band gap that leads to the structural colour.

confirm that the 2D morphologies of the surfaces are well reproduced, as shown in figure 6*d*–*f*.

Finally, the photonic band diagram is calculated for the single-diamond photonic crystal, as shown in figure 8. For the calculation, the refractive index of the cuticle was determined to be 1.515 by the Becke line test, using a series of refractive index liquids (Cargille series A, cat.# 18095). In this measurement, we also found that the scale is almost transparent under the transmission illumination of white light, indicating that the extinction coefficient is approximately zero. The level set parameter t in equation (2.1) was determined to be 0.15 (volume fraction of cuticle 0.53) from the SEM image (figure 3): the areas of the air holes were determined by an image analysis that could be used to estimate the parameter t. By using these values, we calculated the wavelength of the band gap in the Γ-L direction, which was found to range from 557 to 629 nm; this is in good agreement with the reflection band observed with the microspectrophotometer, as shown in figure 2.

5. Discussion

It has been presumed that the natural photonic crystals can be modelled by using the constant mean curvature surfaces, which include the simple cubic, gyroid and diamond surfaces as the simple cases [4,23]. The 3D comparison clearly shows that the observed network topology of *L. augustus* is the single-network diamond type (figure 7), agreeing with the previous study [10]. The single-diamond network structure has been reported for other weevil species *Entimus imperialis* [8] and *Hypera diversipunctata* [7]. On the other hand, a recent SAXS study reported for *L. augustus* that both the diamond and gyroid photonic crystals are found [9]. Although we have not noted very differently coloured scales or regions in a scale from microscopic observation, further structural study is necessary to examine how often such a scale appears and/or how much of the region of the scale has each type of network structure. It is desirable to distinguish the gyroid and diamond structures only from the observation of the surface morphology that can be examined by SEM. One possible way is to focus our attention on the differences in the morphology of the higher-symmetry directions. A sample could be tilted and/or rotated to find ⟨111⟩ orientations, which are easy to find due to its threefold symmetry. If the air holes appear to penetrate the structure from that direction, it implies that the network is the gyroid type, as illustrated in a figure in [13]. If not, the diamond type is implied. Then, the sample is tilted by 33.5° to examine if there are directions with the through-hole feature. If so, that is another indication of the diamond network, as shown in figure 6*b*,*e*.

It is concluded from the structural and optical investigations that ⟨111⟩ orientations are preferred to be along the surface normal of the scale of *L. augustus*. In other words, the scale of this weevil has a highly uniform crystallographic texture. Such a crystallographic texture has been reported probably for the first time in the weevil species. For a different weevil *Eupholus magnificus*, apparently random orientations have been reported [24]. On the other hand, almost uniformly coloured scales have been observed for *Glenea celia* and *Pachyrhynchus moniliferus* [25]. Thus, the degree of the crystallographic texture may vary, largely depending on the weevil species.

Recently, the development of the gyroid crystallites in the butterfly wing scale has been discussed in terms of the nucleation and growth processes by taking advantage of the domain size gradient within a scale [14]. If such processes are the case for this weevil scale, there must be some factors regulating the crystal orientation when the nuclei appear. The photonic crystals in the butterfly and weevil are different in the surrounding

structure. The photonic crystal of the butterfly wing scale exists on the lower laminae and is covered by highly decorated upper structures such as ridges and cross ribs, while the photonic crystal of the weevil scale seems to be contained in a flattened sac of the cuticle layer. It is hypothesized for the butterfly wing scale that the nuclei appear on the upper structure because the crystals are attached to it [14]. If the nuclei are assumed to appear on both the lower and upper laminae in the weevil, it may explain an observation in a weevil *E. magnificus* that the adjacent crystal domains are occasionally vertically overlapped rather than horizontally attached [24]. However, such overlapped domains are not observed in *L. augustus*. This difference may be related to the fact that the scale of *L. augustus* is thinner than that of *E. magnificus*; the scale of the latter species is slightly bulged so that the photonic crystal layer becomes thick.

Another structural factor that is very different among species is the size of the crystal domains; the crystal domains have been observed to be very large in the weevil *Entimus imperialis* such that there are only a few domains in one scale [21]. Thus, the photonic crystal structures in the weevil scale are different, depending on the species, at least, in the size of the crystal domain, configurations of the crystals (overlapping), and degree of the crystallographic texture. A comprehensive study on these morphological differences will give us information for understanding the development of the photonic crystal structure.

The filling ratio of the cuticle is related to the ratio of the band gap and mid-gap frequency. It has been reported for a butterfly species that the cuticle filling ratio is located nearly at the position that maximizes the ratio of the band gap and mid-gap frequency [26]. On the other hand, the filling ratio of 0.3 in a weevil *E. imperialis* has been found to be less than the optimal value 0.4 [21]. In this study, the filling ratio of 0.53 of *L. augustus* is found to be more than the optimal value. However, the ratio of the band gap and mid-gap frequency does not form a sharp peak against the cuticle fraction, but a rather broad one [21]. Thus, the amount of the cuticle fraction may not be under severe selection pressure during the evolution. However, it may be used to adjust the wavelength of the reflection (colour) without significantly affecting the magnitude of the reflection.

Data accessibility. This article has no additional data.

Authors' contributions. All authors participated in the design of the project. H.H., J.K. and T.F. considered the methods for structural characterization. R.E. performed experiments. R.E. and S.Y. analysed the results and wrote the paper.

Competing interests. We declare we have no competing interests.

Funding. This work was supported by a Grant-in-Aid for Scientific Research Nos 22340121, 24120004 on Innovative Areas: 'Engineering Neo-Biomimetics' (Area no. 4402), and No. 18H01191 from the Ministry of Education, Culture, Sports, Science, and Technology (MEXT, Japan). The sequential FIB milling and SEM imaging was carried out on the 'Nanotechnology Platform Japan' programme sponsored by the MEXT.

Acknowledgements. We thank Dr Kiyomi Nakajima for the assistance with FIB milling and SEM imaging.

References

1. Seago AE, Brady P, Vigneron J-P, Schultz TD. 2009 Gold bugs and beyond: a review of iridescence and structural colour mechanisms in beetles (Coleoptera). *J. R. Soc. Interface* **6**, S165–S184. (doi:10.1098/rsif.2008.0354.focus)
2. Biro L, Vigneron J. 2011 Photonic nanoarchitectures in butterflies and beetles: valuable sources for bioinspiration. *Laser Photonics Rev.* **5**, 27–51. (doi:10.1002/lpor.200900018)
3. Joannopoulos JD, Johnson SG, Winn JN, Meade RD. 2008 *Photonic Crystals: Molding the Flow of Light (Second Edition)*. Princeton, NJ: Princeton University Press.
4. Michielsen K, Stavenga D. 2008 Gyroid cuticular structures in butterfly wing scales: biological photonic crystals. *J. R. Soc. Interface* **5**, 85–94. (doi:10.1098/rsif.2007.1065)
5. Saranathan V, Osuji CO, Mochrie SGJ, Noh H, Narayanan S, Sandy A, Dufresne ER, Prum RO. 2010 Structure, function, and self-assembly of single network gyroid ($I4_132$) photonic crystals in butterfly wing scales. *Proc. Natl Acad. Sci. USA* **107**, 11 676–11 681. (doi:10.1073/pnas.0909616107)
6. Schröder-Turk GE, Wickham S, Averdunk H, Brink F, Fitz Gerald JD, Poladian L, Large MCJ, Hyde ST. 2011 The chiral structure of porous chitin within the wing-scales of callophrys rubi. *J. Struct. Biol.* **174**, 290–295.
7. McNamara ME, Saranathan V, Locatelli ER, Noh H, Briggs DEG, Orr PJ, Cao H. 2014 Cryptic iridescence in a fossil weevil generated by single diamond photonic crystals. *J. R. Soc. Interface* **11**, 20140736. (doi:10.1098/rsif.2014.0736)
8. Wilts BD, Michielsen K, Kuipers J, De Raedt H, Stavenga DG. 2012 Brilliant camouflage: photonic crystals in the diamond weevil, entimus imperialis. *Proc. R. Soc. B* **279**, 2524–2530. (doi:10.1098/rspb.2011.2651)
9. Saranathan V, Seago AE, Sandy A, Narayanan S, Mochrie SGJ, Dufresne ER, Cao H, Osuji CO, Prum RO. 2015 Structural diversity of arthropod biophotonic nanostructures spans amphiphilic phase-space. *Nano. Lett.* **15**, 3735–3742. (doi:10.1021/acs.nanolett.5b00201)
10. Galusha JW, Richey LR, Gardner JS, Cha JN, Bartl MH. 2008 Discovery of a diamond-based photonic crystal structure in beetle scales. *Phys. Rev. E* **77**, 050904. (doi:10.1103/PhysRevE.77.050904)
11. Argyros A, Manos S, Large MCJ, McKenzie DR, Cox GC, Dwarte DM. 2002 Electron tomography and computer visualisation of a three-dimensional 'photonic' crystal in a butterfly wing-scale. *Micron* **33**, 483–487.
12. Colomer J-F, Simonis P, Bay A, Cloetens P, Suhonen H, Rassart M, Vandenbem C, Vigneron JP. 2012 Photonic polycrystal in the greenish-white scales of the african longhorn beetle prosopocera lactator (Cerambycidae). *Phys. Rev. E* **85**, 011907. (doi:10.1103/PhysRevE.85.011907)
13. Winter B, Butz B, Dieker C, Schröder-Turk GE, Mecke K, Spiecker E. 2015 Coexistence of both gyroid chiralities in individual butterfly wing scales of callophrys rubi. *Proc. Natl Acad. Sci. USA* **112**, 12 911–12 916. (doi:10.1073/pnas.1511354112)
14. Wilts BD, Apeleo Zubiri B, Klatt MA, Butz B, Fischer MG, Kelly ST, Spiecker E, Steiner U, Schröder-Turk GE. 2017 Butterfly gyroid nanostructures as a time-frozen glimpse of intracellular membrane development. *Sci. Adv.* **3**, e1603119. (doi:10.1126/sciadv.1603119)
15. Maldovan M, Thomas EL. 2004 Diamond-structured photonic crystals. *Nat. Mater.* **3**, 593–600. (doi:10.1038/nmat1201)
16. Johnson SG, Joannopoulos JD. 2000 Three-dimensionally periodic dielectric layered structure with omnidirectional photonic band gap. *Appl. Phys. Lett.* **77**, 3490–3492. (doi:10.1063/1.1328369)
17. Yoshioka S, Fujita H, Kinoshita S, Matsuhana B. 2014 Alignment of crystal orientations of the multi-domain photonic crystals in parides sesostris wing scales. *J. R. Soc. Interface* **11**, 20131029. (doi:10.1098/rsif.2013.1029)
18. Singer A, Boucheron L, Dietze SH, Jensen KE, Vine D, McNulty I, Dufresne ER, Prum RO, Mochrie SGJ, Shpyrko OG. 2016 Domain morphology, boundaries, and topological defects in biophotonic gyroid

nanostructures of butterfly wing scales. *Sci. Adv.* **2**, e1600149. (doi:10.1126/sciadv.1600149)

19. Corkery RW, Tyrode EC. 2017 On the colour of wing scales in butterflies: iridescence and preferred orientation of single gyroid photonic crystals. *Interface Focus* **7**, 29160154. (doi:10.1098/rsfs.2016.0154)
20. Yoshioka S, Matsuhana B, Tanaka S, Inouye Y, Oshima N, Kinoshita S. 2011 Mechanism of variable structural colour in the neon tetra: quantitative evaluation of the venetian blind model. *J. R. Soc. Interface* **8**, 56–66. (doi:10.1098/rsif.2010.0253)
21. Wilts BD, Michielsen K, De Raedt H, Stavenga DG. 2012 Hemispherical brillouin zone imaging of a diamond-type biological photonic crystal. *J. R. Soc. Interface* **9**, 1609–1614. (doi:10.1098/rsif.2011.0730)
22. Ho KM, Chan CT, Soukoulis CM. 1990 Existence of a photonic gap in periodic dielectric structures. *Phys. Rev. Lett.* **65**, 3152–3155. (doi:10.1103/PhysRevLett.65.3152)
23. Wohlgemuth M, Yufa N, Hoffman J, Thomas EL. 2001 Triply periodic bicontinuous cubic microdomain morphologies by symmetries. *Macromolecules* **34**, 6083–6089. (doi:10.1021/ma0019499)
24. Pouya C, Stavenga DG, Vukusic P. 2011 Discovery of ordered and quasi-ordered photonic crystal structures in the scales of the beetle eupholus magnificus. *Opt. Express* **19**, 11 355–11 364. (doi:10.1364/OE.19.011355)
25. Galusha JW, Richey LR, Jorgensen MR, Gardner JS, Bartl MH. 2010 Study of natural photonic crystals in beetle scales and their conversion into inorganic structures via a sol-gel bio-templating route. *J. Mater. Chem.* **20**, 1277–1284. (doi:10.1039/B913217A)
26. Pouya C, Vukusic P. 2012 Electromagnetic characterization of millimetre-scale replicas of the gyroid photonic crystal found in the butterfly *parides sesostris*. *Interface Focus* **2**, 645–650. (doi:10.1098/rsfs.2011.0091)